

1 **CFD simulation of dense gas dispersion in neutral**
2 **atmospheric boundary layer with OpenFOAM**

3 **Vu Tran · E. Y. K. Ng · Martin Skote**

4

5 Received: date / Accepted: date

6 **Abstract** In this study, MOST (Monin-Obukhov Similarity Theory) is used to
7 specify the profiles of velocity, turbulent kinetic energy (k) and eddy dissipa-
8 tion rate (ϵ) in ABL (Atmospheric Boundary Layer) flow. The OpenFOAM stan-
9 dard solver *buoyantSimpleFoam* is modified to simulate neutrally stratified ABL.
10 The solver is able to obtain equilibrium ABL. For gas dispersion simulation,
11 *buoyantNonReactingFoam* is developed to take into accounts fluid properties
12 change due to temperature, buoyancy effect and variable turbulent Schmidt num-
13 ber. The solver is validated for dense gas dispersion in wind tunnel test and field
14 test of LNG (Liquefied Natural Gas) vapour dispersion in neutrally stratified ABL.

15 **Keywords** LNG dispersion · CFD · ABL · OpenFOAM

Vu Tran, E. Y. K. Ng

School of Mechanical and Aerospace Engineering, Nanyang Technological University, Singapore

E-mail: tranlevu001@e.ntu.edu.sg

Martin Skote

School of Aerospace, Transport and Manufacturing, Cranfield University, UK

1 Introduction

Many human activities are affected by the atmospheric boundary layer (ABL). This is also where most air pollution phenomena occur. Understanding of the processes taking place in the ABL has attracted various research studies. Some typical applications of ABL related research topics are wind engineering, urban flows, weather forecast, air pollution and risk assessment of hazardous material spills in industrial sites

One hazardous dense gas is liquefied natural gas (LNG), which is an effective solution for long-distance natural gas transfer. LNG has become the preferred option for international trading of natural gas. However, LNG storage, handling, transportation are exposed to serious risks for humans, equipment and the environment due to thermal hazards associated with combustion events such as pool fire, vapour cloud fire, explosion or rapid phase transition. Safety assessment and hazard mitigation methods should be applied to lower the possibilities of catastrophic disaster relating to the LNG industry. The scope of this study is constrained to the discussion of dense gas dispersion when released into the ABL.

Computational Fluid Dynamics (CFD) is increasingly being used in simulation of ABL flows. Open source CFD tool is a more powerful research tool in comparison to proprietary software because of its flexibility to incorporate new implementation of fields calculation and post-processing. OpenFOAM is an open source CFD software package that attracts users from both industry and academia. Using a general CFD code such as OpenFOAM for simulating ABL flow and gas dispersion also encourages research sharing and reusing code in this specific field where in-house code is usually adopted.

40 An important task before modelling gas dispersion in the ABL is obtaining
41 the correct ABL flow prior to the release of gas source. One approach to achieve
42 this is using equilibrium ABL, i.e. zero stream-wise gradients of all variables, as
43 a steady state ABL flow. For neutral ABL, Richards and Hoxey (1993) proposed
44 appropriate boundary conditions of mean wind speed and turbulence quantities
45 for the standard $k - \epsilon$ model based on Monin-Obukhov similarity theory (MOST).
46 These profiles were derived assuming constant shear stress with height and were
47 used to model ABL as horizontally homogeneous turbulent surface layer (HHTSL).
48 However, HHTSL was hard to achieve mostly due to the ground boundary condi-
49 tions (Yang et al., 2009), which manifested in a decay of velocity profile due to a
50 spike in the turbulent kinetic energy close to the ground. However, consistency be-
51 tween wall boundary conditions, turbulence model with associated constants and
52 numerical schemes was shown to achieve HHTSL (Jonathon and Christian, 2012;
53 Parente et al., 2011; Yan et al., 2016). These authors adopted proprietary CFD
54 software for their simulation. Applying these implementations in open-source CFD
55 code also require extensive modifications of the source code to successfully simu-
56 late equilibrium ABL. OpenFOAM was previously used for atmospheric buoyant
57 (Flores et al., 2013) and dense gas dispersions (Mack and Spruijt, 2013; Fiates
58 et al., 2016; Fiates and Vianna, 2016). However, the validation of these solvers
59 in simulation of equilibrium ABL was not reported. Therefore, the atmospheric
60 turbulence might not be correctly solved throughout the computational domain.

61 In this study, MOST is used to model the profiles of velocity, turbulent kinetic
62 energy (k) and eddy dissipation rate (ϵ) of ABL according to an approach proposed
63 by Richards and Hoxey (1993). These profiles are used as the boundary conditions
64 at the inlet of ABL flow simulation. OpenFOAM application `buoyantSimpleFoam`

65 is modified to simulate neutrally stratified ABL turbulence. For gas dispersion
 66 simulation, `buoyantNonReactingPimpleFoam` is developed to take into account the
 67 buoyancy effect and variable turbulent Schmidt number. The solver is validated
 68 for dense gas dispersion cases from wind tunnel and field tests of LNG vapour
 69 dispersion in neutrally stratified ABL.

70 2 Methodology

71 2.1 Models

72 The $k - \epsilon$ model is used for turbulence modelling. It is based on expression of
 73 turbulent dynamic viscosity μ_t by Jones and Launder (1972):

$$\mu_t = \rho C_\mu \frac{k^2}{\epsilon} \quad (1)$$

74 Two additional transport equations for turbulence kinetic energy k and tur-
 75 bulence dissipation rate ϵ are required. To include the effect of buoyancy, the
 76 transport equations for k and ϵ are:

$$\frac{D}{Dt}(\rho k) = \frac{\partial}{\partial x_i} \left[\left(\mu + \frac{\mu_t}{\sigma_k} \right) \frac{\partial k}{\partial x_j} \right] + G_k + G_b - \rho \epsilon \quad (2)$$

$$\frac{D}{Dt}(\rho \epsilon) = \frac{\partial}{\partial x_i} \left[\left(\mu + \frac{\mu_t}{\sigma_\epsilon} \right) \frac{\partial \epsilon}{\partial x_j} \right] + C_{1\epsilon} \frac{\epsilon}{k} G_k + C_{1\epsilon} C_{3\epsilon} \frac{\epsilon}{k} G_b - C_{2\epsilon} \rho \frac{\epsilon^2}{k} \quad (3)$$

77 where ρ is the fluid density; $C_\mu = 0.09$, $\sigma_k = 1$, $\sigma_\epsilon = 1.3$, $C_{1\epsilon} = 1.44$ and $C_{2\epsilon} =$
 78 1.92 are model constants as proposed in original paper (Launder and Spalding,
 79 1974). The value of $C_{3\epsilon}$ is calculated using:

$$C_{3\epsilon} = \tanh \left| \frac{v}{u} \right| \quad (4)$$

80 where v , u are vertical and horizontal velocity accordingly.

81 G_k is production of turbulence kinetic energy due to the mean velocity gradi-
82 ents. G_b is the buoyancy source term:

$$G_b = -\frac{\mu_t}{\rho Pr_t} (\mathbf{g} \cdot \nabla \rho) = -C_g \frac{\mu_t}{\rho} (\mathbf{g} \cdot \nabla \rho) \quad (5)$$

83 where $C_g = 1/Pr_t$ is used as a model constant to take into account the user-
84 defined value of turbulent Prandtl number Pr_t . \mathbf{g} is gravitational vector.

85 Energy, heat and transport properties are determined by a set of thermophys-
86 ical models (Greenshields, 2017) in OpenFOAM. This set defines mixture type,
87 transport and thermodynamic properties models, choice of energy equation vari-
88 able and equation of states.

89 The fluid in a simulation is defined as a mixture of fixed compositions. Enthalpy
90 is chosen as energy equation variable. Transport and thermodynamic properties
91 are determined using models based on the density ρ , which are calculated from
92 pressure and temperature fields. Polynomial functions of order N are used to relate
93 transport property μ , the specific heat c_p and density ρ with temperature field T :

$$\begin{aligned} \mu &= \sum_i^{N-1} a_{\mu i} T^i \\ c_p &= \sum_i^{N-1} a_{c_p i} T^i \\ \rho &= \sum_i^{N-1} a_{\rho i} T^i \end{aligned} \quad (6)$$

94 where $a_{\mu i}$, $a_{c_p i}$ and $a_{\rho i}$ are the polynomials coefficients.

95 2.2 Boundary conditions

96 2.2.1 ABL air inlet

97 MOST has been validated for the surface layer of ABL by many empirical stud-
 98 ies (Foken, 2006). It assumes horizontally homogeneous and quasi-stationary flow
 99 field, i.e. profiles of flow variables are only varying in the vertical direction and
 100 their vertical fluxes are assumed constant. The inlet boundary conditions proposed
 101 by Richards and Hoxey (1993) based on MOST are widely used in CFD study of
 102 atmospheric flow. The velocity, turbulent production rate k and dissipation rate ϵ
 103 profiles in vertical direction z are written as:

$$\begin{aligned}
 u(z) &= \frac{u_*}{\kappa} \ln \frac{z + z_0}{z_0} \\
 k &= \frac{u_*^2}{\sqrt{C_\mu}} \\
 \epsilon(z) &= \frac{u_*^3}{\kappa(z + z_0)}
 \end{aligned}
 \tag{7}$$

104 where z_0 is aerodynamic roughness length, u_* is friction velocity, C_μ is $k - \epsilon$
 105 model constant.

106 These profiles are implemented in OpenFOAM as `atmBoundaryLayer` class and
 107 its subclasses. Required parameters are flow and vertical direction, reference ve-
 108 locity, reference height and aerodynamic roughness length. The friction velocity is
 109 calculated as:

$$u_* = \frac{\kappa * u_{ref}}{\ln((z_{ref} + z_0)/z_0)}
 \tag{8}$$

110 Parente et al. (2011) presented an elaborate procedure to ensure the consistency
 111 for arbitrary inlet profile of turbulent kinetic energy k . Instead of altering model

112 constants as Yang et al. (2009), the effect of non-constant k on momentum and ϵ
 113 equation can be characterised by deriving an equation for C_μ :

$$C_\mu(z) = \frac{u_*^4}{k(z)^2} \quad (9)$$

114 Source terms are added to k and ϵ transport equations to ensure equilibrium
 115 condition:

$$\begin{aligned} S_k &= \frac{\rho u_* \kappa}{\sigma_k} \frac{\partial}{\partial z} \left((z + z_0) \frac{\partial k}{\partial z} \right) \\ S_\epsilon &= \frac{\rho u_*^4}{(z + z_0)^2} \left[\frac{(C_{\epsilon 2} - C_{\epsilon 1}) \sqrt{C_\mu}}{\kappa^2} - \frac{1}{\sigma_\epsilon} \right] \end{aligned} \quad (10)$$

116 Richards and Norris (2011) revisited the problem of modelling the HHTSL by
 117 deriving the inlet profiles directly from the conservation and equilibrium equations.
 118 This allows various inlet profiles to be specified by varying the turbulence model
 119 constants. For standard $k - \epsilon$ models, the inlet profiles of velocity and turbulence
 120 properties are identical to Equation (7). However they suggested to change the
 121 von-Karman constant κ according to model constants as:

$$\kappa = \sqrt{(C_{\epsilon 2} - C_{\epsilon 1}) \sigma_\epsilon \sqrt{C_\mu}} \quad (11)$$

122 Using the standard $k - \epsilon$ model constants, we obtain $\kappa_{k-\epsilon} = 0.433$.

123 2.2.2 Wall boundary conditions

124 In CFD, the below approximation is used to calculate wall shear stress:

$$\tau_w = \nu_t \frac{\partial u}{\partial n} \Big|_w \approx \nu_t \frac{(u_P - u_w)}{y_P} \quad (12)$$

125 where y_P is distance to wall of the wall adjacent cell. Subscript w and P denote
 126 field value evaluated at wall and wall adjacent point respectively.

127 However, this approximation is inaccurate when wall velocity gradient is signif-
 128 icantly larger than velocity difference between the adjacent cell and the wall. This
 129 is the case for most ABL flows. Turbulent kinematic viscosity ν_t wall function is
 130 used to calculate the wall shear stress τ_w from the wall velocity difference. To take
 131 into account the aerodynamic roughness length z_0 , the calculation of turbulent
 132 kinematic viscosity at wall adjacent cell is:

$$\nu_t = \frac{\kappa u_* y_P}{\ln\left(\frac{y_P + z_0}{z_0}\right)} \quad (13)$$

133 where friction velocity u_* can be calculated from a simple relation derived by
 134 Launder and Spalding (1974), assuming that generation and dissipation of energy
 135 are in balance:

$$u_* = C_\mu^{1/4} k^{1/2} \quad (14)$$

136 ϵ wall function is used to calculate value of ϵ at wall adjacent cell ϵ_P as:

$$\epsilon_P = \frac{C_\mu^{0.75} k^{1.5}}{\kappa y_P + z_0} \quad (15)$$

137 The wall is usually defined as non-slip condition where velocity is zero. How-
 138 ever, to account for the effect of aerodynamic roughness length, a new boundary
 139 condition for velocity is implemented in OpenFOAM as:

$$u_P = \frac{u_*}{\kappa} \ln\left(\frac{y_P + z_0}{z_0}\right) \quad (16)$$

140 2.2.3 Top, side and outlet boundaries

141 At the outlet boundary, the flow is assumed fully developed and unidirectional.

142 All flow variables are supposed to be constant at this boundary.

143 The top and side of the computational domain are external boundaries repre-
 144 senting the far fields of flow. If a constant pressure is applied in these boundaries,
 145 this may alter the inlet wind profile in case the prescribed pressure is not matched
 146 with the boundary velocity (Luketa-Hanlin et al., 2007). The zero gradient bound-
 147 ary condition, which set normal velocity to zero and all others variables are set
 148 equal to the inner values, or symmetry condition can be used at the top and side
 149 boundaries to reserve the wind profile and eliminate the effect of changing the
 150 inlet profiles.

151 Hargreaves and Wright (2007) showed that zero gradient velocity at the top
 152 boundary resulted in a decay of velocity downstream, due to the extraction of
 153 energy at the wall with respect to the wall shear stress. A driving shear stress,
 154 zero flux of turbulent kinetic energy and a flux of dissipation rate ϵ are imposed
 155 at the upper boundary:

$$\begin{aligned} \frac{du}{dz} &= \frac{u_*}{\kappa z} \\ \frac{\mu_t}{\sigma_\epsilon} \frac{d\epsilon}{dz} &= -\frac{\rho u_*^4}{\sigma_\epsilon z} \end{aligned} \quad (17)$$

156 2.3 Numerical tool and data sets

157 OpenFOAM is an open source CFD software package based on finite volume

158 method, co-located variables and unstructured polyhedral meshes. In this study,

159 `buoyantSimpleFoam` is used to simulate ABL turbulence. The application `buoyantNonReactingFoam`

160 is developed based on `rhoReactingBuoyantFoam` solver, previously used for dense
161 gas dispersion by Fiates et al. (2016), to simulate atmospheric turbulence un-
162 der neutral stability for dispersion of dense gas continuous source in flat terrain.
163 `buoyantNonReactingFoam` uses polynomial thermophysical models to account for
164 the change of fluid properties due to temperature. The solver takes into account
165 the buoyancy effect and the variable turbulent Schmidt number. Algorithms used
166 in these two solvers are presented in Algorithm 1 and 2.

Algorithm 1 `buoyantSimpleFoam` solver algorithm

- 1: Initializing variables such as: time variables, mesh, solution control, fields and continuity errors
 - 2: **while** $t < t_{end}$ **do**
 - 3: Solving momentum equation
 - 4: Solving energy equation for enthalpy and correcting thermal properties
 - 5: Solving pressure correction equation for p_{rgh} and calculating pressure field
 - 6: Correcting turbulent properties
 - 7: Writing fields
 - 8: **end while**
-

Algorithm 2 buoyantNonReactingFoam solver algorithm

```
1: Initializing variables such as: time variables, mesh, solution control, fields and continuity
   errors
2: while  $t < t_{end}$  do
3:    $t+ = \Delta t$ 
4:   Solving continuity equation for density
5:   while PIMPLE outer correctors do
6:     Solving momentum equation
7:     Solving species transport equation
8:     Solving energy equation for enthalpy and correcting thermal properties
9:     while PIMPLE inner correctors do
10:      Solving pressure correction equation for  $p_{rgh}$  and calculating pressure field
11:      Solving continuity equation for density
12:      Calculating time step continuity errors
13:     end while
14:     Correcting turbulent properties
15:   end while
16:   Writing fields
17: end while
```

167 Boundary conditions used for ABL flows are developed as new libraries in
168 OpenFOAM. These include velocity inlet, turbulent kinetic energy, dissipation
169 rate inlet and wall boundary conditions.

170 A set of full scale field tests and experimental wind tunnel tests for LNG dis-
171 persion model validation was reported in (Ivings et al., 2013). Most data of these
172 tests were available in REDIPHEM database (Nielsen and Ott, 1996). The data
173 contains physical comparison parameters of each test. These are maximum arc-
174 wise concentration, i.e. the maximum concentration across an arc at the specified

175 distance from the source and point-wise concentration, i.e. the concentration at
 176 specific sensor locations. Two wind tunnel data DA0120 and DAT223 are used to
 177 validate OpenFOAM solver in prediction of dense gas dispersion over a flat, un-
 178 obstructed terrain in simulated neutral ABL. In these tests, continuous source of
 179 SF₆ gas was released in flat terrain without obstructions. For field test, we select
 180 **Burro9**, which is continuous LNG spills under neutral ABL.

181 **3 Neutral ABL simulation**

182 3.1 Domain and mesh

183 A 2D domain of 5000 m × 500 m with the resolution of 500 × 50 cells is used for the
 184 simulation of neutral ABL over flat terrain. The mesh is uniform in stream-wise
 185 direction and stretched in vertical direction with the expansion ratio of 1.075.

186 3.2 Numerical setting

187 The boundary conditions of the cases are represented in Table 1.

Table 1 Boundary conditions for neutral ABL simulation

ABL inlet	profiles of k , u , ϵ	Eq. (7)
ABL outlet	zeroGradient for all variables fixedValue for static pressure	
ABL side	zeroGradient for all variables	
ABL top	zeroGradient for all variables fixedFlux/zeroGradient for u and ϵ	Eq. (17)
ABL bottom	noSlip for u	

188 ABL parameters used to define inlet variable profiles are listed in Table 2
 189 according to the reference case of Hargreaves and Wright (2007):

Table 2 ABL parameters using for neutral ABL simulation

u_* (m/s)	z_0 (m)	u_{ref} (m/s)	z_{ref} (m)
0.625	0.01	10	6

190 Steady state simulation is employed using `buoyantNonReactingSimpleFoam` de-
 191 scribed in previous section. OpenFOAM discretisation schemes, velocity-pressure
 192 coupling algorithm as well as linear solvers are listed below:

- 193 – Time schemes: `steadyState`
- 194 – Gradient schemes: `Gauss linear`
- 195 – Divergence schemes: `Gauss limitedLinear 1`
- 196 – Surface normal gradient schemes: `corrected`
- 197 – Laplacian schemes: `Gauss linear corrected`
- 198 – Interpolation schemes: `linear`
- 199 – Solving algorithm: `SIMPLE`
- 200 – Linear solver for p: `GAMG` with `DICGaussSeidel` preconditioner
- 201 – Linear solver for U, h, k, epsilon: `PBiCGStab` with `DILU` preconditioner

202 Residual control is set at three order of magnitude for pressure and four order
 203 of magnitude for other variables such as U , k , ϵ and h . Modification of $k - \epsilon$
 204 (Equation (11)) are used to simulate neutral ABL and comparing with standard
 205 models. These three cases are summarised in Table 3

206 Different levels of inlet kinetic energy are obtained by altering C_μ according
 207 to Equation (9). The source term by Pontiggia et al. (2009) is implemented us-

Table 3 Turbulence models setting for neutral ABL simulation

Turbulence model	<code>standard $k - \epsilon$</code>	Eq. (10)
	<code>modified $k - \epsilon$</code>	
Wall functions	<code>nutkWallFunction</code> for ν_t	
	<code>epsilonWallFunction</code> for ϵ	
	<code>kqRWallFunction</code> for k	

208 ing Equation (10). Two values of default value $C_\mu = 0.09$ and $C_\mu = 0.017$ are
 209 simulated and compared with Monin-Obukhov theory.

210 3.3 Results and discussion of neutral ABL simulations

211 Modification of $k - \epsilon$ models achieve the matched results as shown in Figure 1.
 212 Including source terms as in Equation (10) is sufficient to compensate terms deflec-
 213 tion from calculation of von-Karman constant $\kappa_{k-\epsilon} = 4.3$ from model constants
 214 (Equation (11)) and $\kappa = 4.1$ used in Monin-Obukhov theory.

215 Results from modelling different turbulence kinetic energy by varying C_μ are
 216 presented in Figure 2. The profiles of velocity and dissipation rate are perfectly
 217 matched with the Monin-Obukhov profiles. In the $C_\mu = 0.017$ simulation, the
 218 value of k near ground is smaller than the theoretical value, however, the kinetic
 219 energy level is matched with the theory at greater height. The smaller value of k at
 220 the wall adjacent cell is due to the wall function, where wall treatment used with
 221 the default $C_\mu = 0.09$ is implemented. However, the overall results are acceptable
 222 for verifying the proposed model in simulating different levels of kinetic energy.

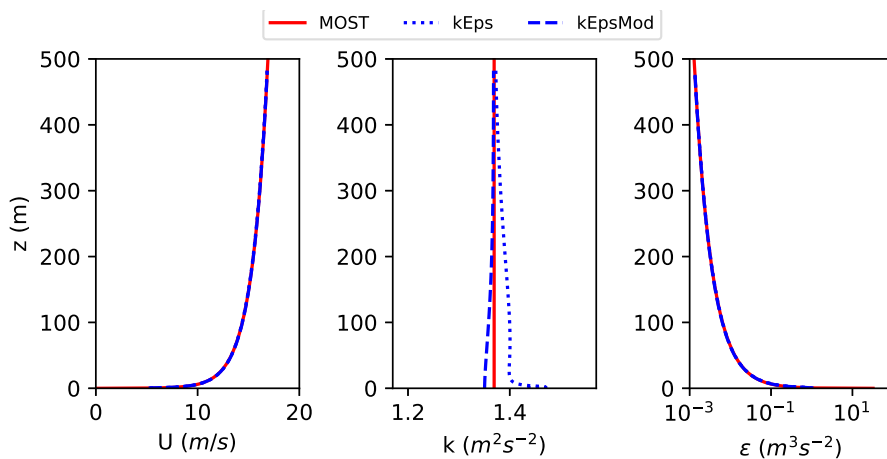


Fig. 1 Comparing velocity, turbulent kinetic energy and turbulent dissipation rate profiles at the outlet boundary from simulation of neutral ABL using standard $k - \epsilon$ (kEps), modified $k - \epsilon$ (kEpsMod) turbulence model and MOST inlet profiles (MOST)

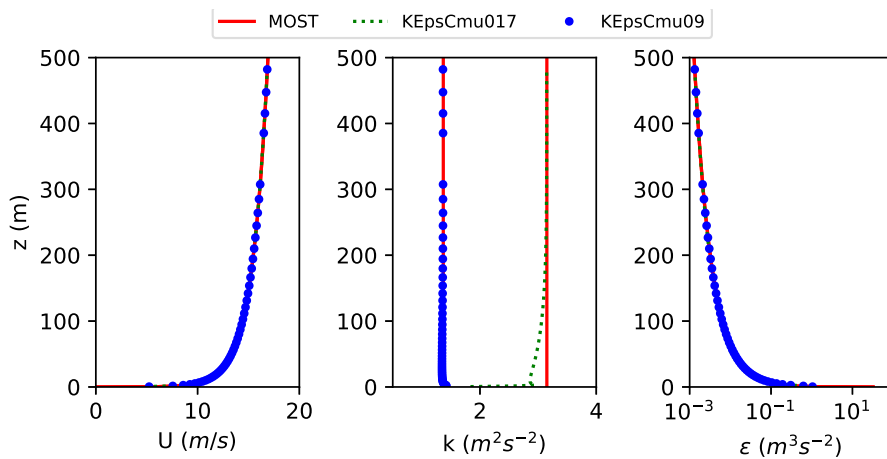


Fig. 2 Comparing velocity, turbulent kinetic energy and turbulent dissipation rate profiles from simulations of different kinetic energy levels by varying $C_\mu = 0.09$ (KEpsCmu09) $C_\mu = 0.017$ (KEpsCmu017) and MOST inlet profiles (MOST)

223 4 Dense gas dispersion in wind tunnel tests

224 4.1 Numerical setting

225 The effect of the turbulent Schmidt number Sc_t is investigated in dense gas disper-
 226 sion. Three test cases are summarised in Table 4. The effect of turbulent models is
 227 examined by applying the modified $k - \epsilon$ which is already validated in simulating
 228 ABL over flat terrain in Section 3.

Table 4 Turbulent Schmidt number Sc_t in Hamburg tests

	Case 1	Case 2	Case 3
Sc_t	1	0.7	0.3
Label (Fig. 4, 10)	FOAM_ORIG	FOAM_Sc07	FOAM_Sc03

229 Firstly, the steady simulation using `bouyantSimpleFoam` is performed to estab-
 230 lish the steady ABL flow prior to the dense gas release. The solver which includes
 231 buoyancy effects `bouyantSimpleFoam` is used to account for of density stratifica-
 232 tion in dense gas flow. The atmospheric inlet profiles are specified by MOST with
 233 parameters in Table 5. Standard $k - \epsilon$ with modifications is used to study the
 234 ability to simulate the ABL with each model. Secondly, the transient simulation
 235 is performed using steady simulation solutions as initial fields. A modified version
 236 of `rhoReactingBouyantFoam` is studied to model multi-species flow where mixture
 237 considered are air and dense gas SF_6 . The wind tunnel tests were conducted in
 238 isothermal condition, therefore constant thermal and transport properties are used
 239 for both gases.

Table 5 Hamburg flat, unobstructed test case parameters (Nielsen and Ott, 1996)

	Unit	DA0120	DAT223
Substance		SF ₆	SF ₆
Density	kg/m ³	6.27	6.27
z_0	m	0.0001	0.0001
Wind speed	m/s	0.54	0.74
Reference height	m	0.00718	0.01367
Ambient temperature	^o C	20	20
Source diameter	m	0.07	0.07
Spill rate	kg/s	0.0001743	0.000872

240 In simulations of DA0120 and DAT223 tests, the discretisation schemes and linear
 241 solver setting are identical to the simulation of neutral ABL (Section 3).

242 4.2 Results and discussion of gas dispersion in wind tunnel tests

243 4.2.1 Peak concentration prediction

244 The steady state plumes at ground level of DAT0120 and DAT223 tests are plotted
 245 in Figure 3. Under higher release volume flow rate and higher wind speed, DAT223
 246 plume is wider and is spreading further downstream than the DAT0120 plume.

247 The predicted and measured peak gas concentration are compared at several
 248 distances from the spill in Figure 4. Turbulent Schmidt number Sc_t has significant
 249 effect in predicting dense gas dispersion. The original `rhoReactingBouyantFoam`
 250 code, with assumption of species diffusivity equals to viscosity, is shown to over-
 251 predict concentration with a factor of three. The modified code takes into account
 252 the variable species diffusivity Sc_t by reading this parameter from user input. The

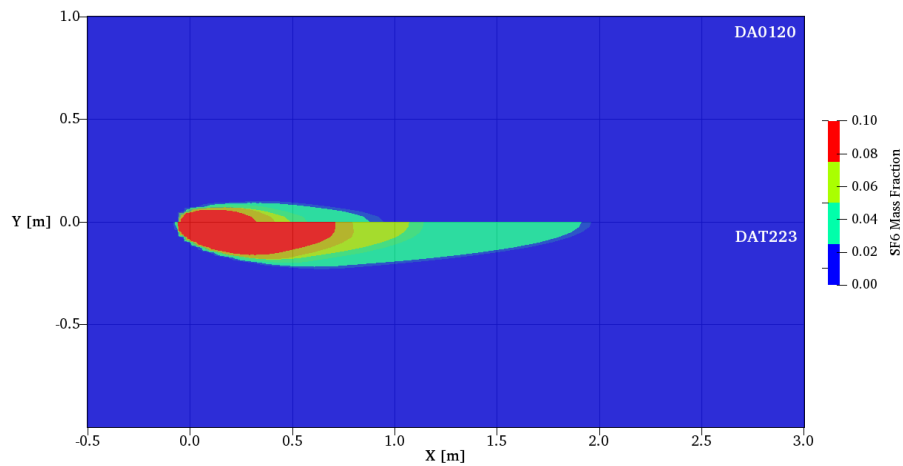


Fig. 3 DA0120(up) and DAT223(below) ground level contours of SF₆ mass fraction

253 value of $Sc_t = 0.3$ is shown to yield a perfect match with the experimental data.
 254 However, there is a slightly acceptable over-predicted species concentration at a
 255 point near the source release.

256 Results from the DAT223 simulation are presented in Figure 5. Satisfactory over
 257 predicted peak concentration is similar to DA0120 case.

258 4.2.2 Point-wise concentration

259 Figure 6 presents gas concentration at the downwind distance $X = 1.84$ of the
 260 DA0120 test. The simulation can reproduce the averaged gas concentration. The
 261 first incidence time of gas concentration is earlier than observed in experiments.
 262 However, the time for reaching averaged maximum concentration is well predicted.

263 4.2.3 Statistical model evaluation

264 Statistical Performance Measures (SPMs) are means to compare prediction param-
 265 eters and the measured ones for model evaluation. The SPM chosen should reflect

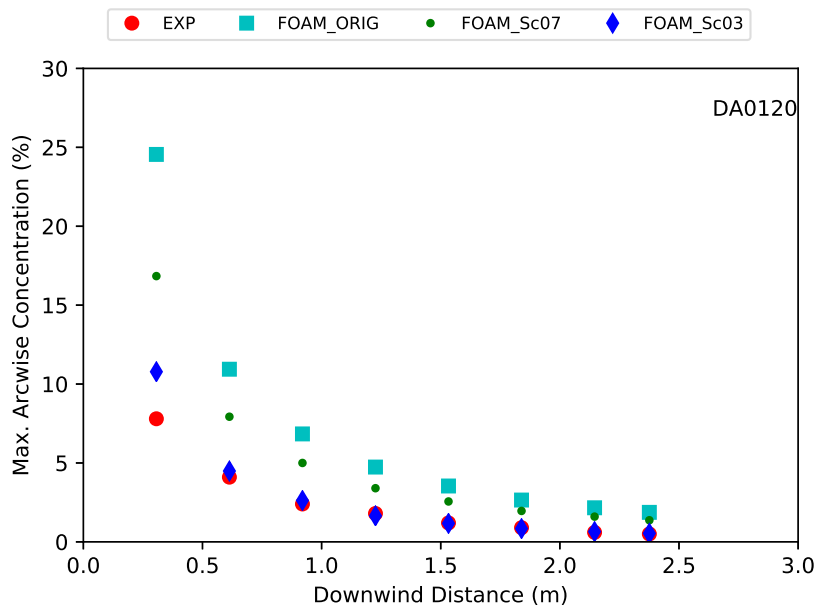


Fig. 4 Peak concentration for DA0120 test

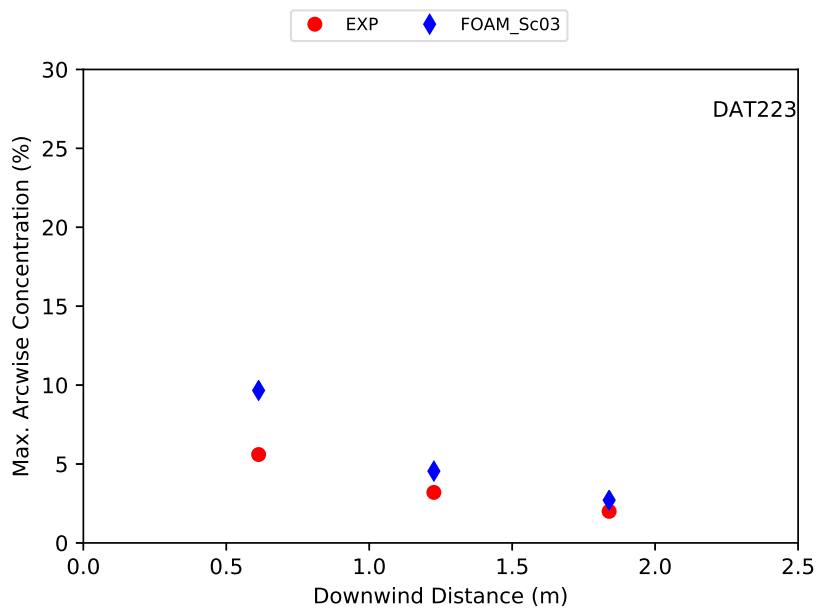


Fig. 5 Peak concentration for DAT223 test

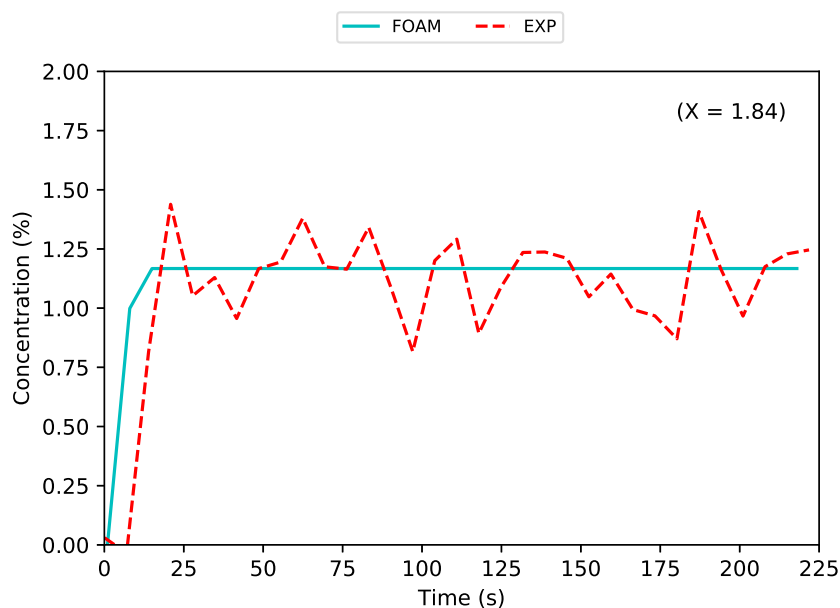


Fig. 6 Concentration at $X = 1.84$ of DA0120 test

266 the bias of these predictions. In the context of LNG vapour dispersion model evalu-
 267 ation, Ivings et al. (2013) proposed five SPMs including mean relative bias (MRB),
 268 mean relative square error (MRSE), the fraction of predictions within the factor of
 269 two of measurements (FAC2), geometric mean bias (MG) and geometric variance
 270 (VG). Definition and acceptability criteria for each SPMs are presented in tabular
 271 form as Table 6 where C_m , C_p are the measured and simulated concentration,
 272 respectively, and \bar{A} denotes the mean operation of variable A .

273 Statistical performance of OpenFOAM results are compared with the spe-
 274 cialised commercial code for gas dispersion FLACS in Table 6. FLACS results
 275 are extracted from (Hansen et al., 2010). The performance of current OpenFOAM
 276 code is considerably better than FLACS. In fact, FLACS is based on the porosity
 277 distributed resistance (PDR) approach. Therefore, this modelling of the boundary
 278 layer close to solid surfaces might contribute to the outperformance of the Open-

279 FOAM model in the comparison. In conclusion, even though larger tests were
 280 validated in FLACS, the proposed model in OpenFOAM is a promising tool for
 281 further investigation of atmospheric dense gas dispersion.

Table 6 Statistical performance measures of Hamburg unobstructed tests

SPM	MRB	RMSE	FAC2	MG	VG
Definition	$\left(\frac{C_m - C_p}{0.5(C_m - C_p)}\right)$	$\left(\frac{(C_m - C_p)^2}{0.25(C_m + C_p)^2}\right)$	$\frac{C_m}{C_p}$	$\exp\left(\ln \frac{C_m}{C_p}\right)$	$\exp\left(\left(\ln \frac{C_m}{C_p}\right)^2\right)$
Acceptable range	[-0.4,0.4]	< 2.3	[0.5, 2]	[0.67, 1.5]	< 3.3
Perfect value	0	0	1	1	1
FLACS (Hansen et al., 2010)	0.25	0.29	0.89	1.34	1.61
<i>FOAM</i>	-0.06	0.02	1.07	1.06	1.02

282 5 LNG vapour dispersion in field tests

283 5.1 Numerical setting

284 The steady simulation uses the atmospheric inlet specified by MOST. Standard
 285 $k-\epsilon$ with modifications is used to study the ability to simulate the ABL with each
 286 model. All required meteorological parameters are tabulated in Table 7, where u_{ref}
 287 and T_{ref} are air velocity and temperature at the height of 2 m respectively.

288 The transient simulation is divided into two steps. The first step is during the
 289 spill duration, i.e. from the time of zero to when the spill ends. The second step
 290 is after the spill stops to the end time of simulation . The gas inlet is treated as a
 291 ground boundary in this later step.

292 The gas inlet condition is usually obtained from separate source term mod-
 293 elling. There is not much information about the vaporisation of LNG from the ex-

294 perimental data. Therefore, uncertainty arises at the setting of this condition. Mass
 295 flux of LNG or the LNG vaporization rate is used to derive source term of LNG
 296 spilling. Luketa-Hanlin et al. (2007) reviewed a number of experiments conducted
 297 to estimate the LNG vaporization rate of the spill on water, the range of this value
 298 varied between approximately 0.029 to $0.195 \text{ kg m}^{-2} \text{ s}^{-1}$. In the case of Burro test,
 299 the simulated vaporisation rate is assumed to be $m''_{LNG} = 0.167 \text{ kg m}^{-2} \text{ s}^{-1}$. Den-
 300 sity of LNG vapour is similar to that of CH_4 at boiling point $\rho_{LNG} = 1.76 \text{ kg m}^{-3}$
 301 (Luketa-Hanlin et al., 2007). The spill diameter is derived from the vaporization
 302 rate, reported spill mass m_{spill} and duration t_{spill} :

$$D_{spill} = \sqrt{\frac{4m_{spill}}{\pi m''_{LNG} t_{spill}}} \quad (18)$$

303 The volume spill rate is used as gas inlet condition:

$$\dot{V}_{spill} = \frac{m_{spill}}{\rho_{LNG} t_{spill}} \quad (19)$$

304 The LNG spill variables used in simulation are also tabulated in Table 7.

Table 7 Burro9 tests meteorological and gas release parameters

Parameters	u_{ref}	u_*	z_0	T_{ref}	t_{spill}	D_{spill}	\dot{V}_{spill}
Unit	m/s	m	m/s	K	s	m	m^3/s
	5.7	0.252	2E-4	308.55	79	32.2	77.17

305 5.2 Results and discussion of LNG vapour dispersion

306 5.2.1 The steady simulation

307 Profiles of velocity and turbulence quantities are sampled at the `outlet` bound-
 308 ary and compared with Monin-Obukhov theory profiles which are used as inlet
 309 boundary conditions. The steady state simulation of ABL with $k - \epsilon$ reveals that
 310 wind velocity and turbulence profiles are accurately reproduced as presented in
 311 Figure 7. The success of the modified $k - \epsilon$ model proves that the proposed model
 312 can adequately reproduce the Monin-Obukhov ABL profiles in the full scale sim-
 313 ulation.

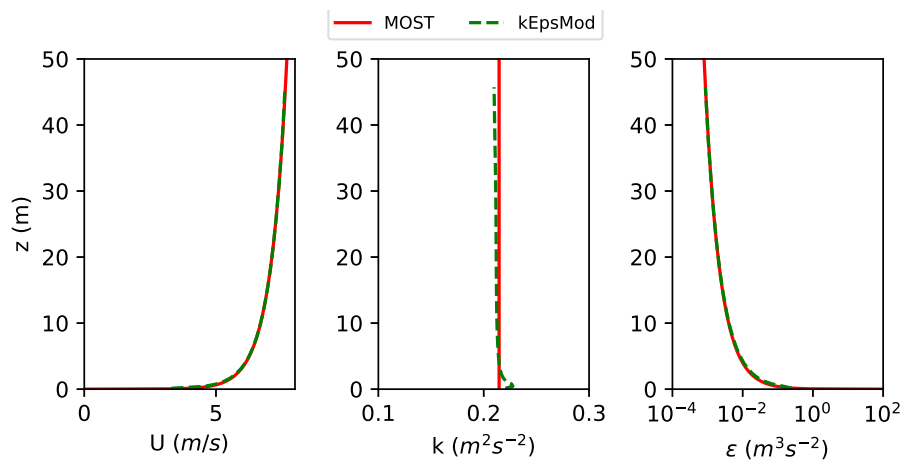


Fig. 7 Comparing ABL profiles at outlet boundary of Burro9 simulation using modified $k - \epsilon$ model (kEpsMod) and MOST inlet profiles (MOST)

314 5.2.2 Mesh sensitivity study

315 Maximum concentration at the arcs of 57 m, 140 m, 400 m and 800 m downwind
 316 are used as performance parameters for the mesh sensitivity study. Three meshes

317 with refined factors as summarised in Table 8 are used to simulate LNG gas dis-
 318 persion under adiabatic thermal wall condition. Results from four peak arc-wise
 319 concentrations are plotted in Figure 8.

Table 8 Burro test computational domain and mesh parameters

	Mesh 1	Mesh 2	Mesh 3
Domain region	[(-150, 0, 50), (850, 300, 50)]		
Refined region	[(-100, 0, 5), (400, 100, 5)]		
Mesh size (m)	10	5	2
Mesh refined size (m)	5	2	1

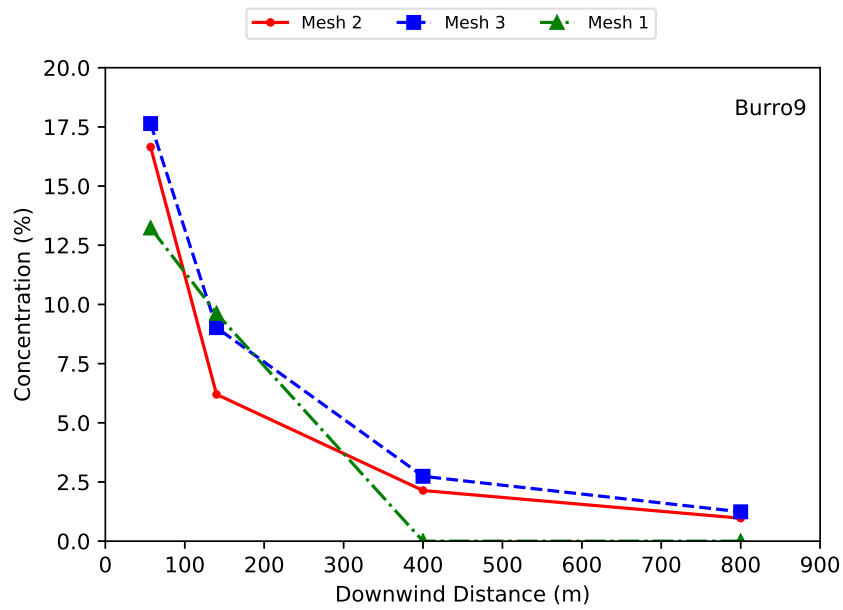


Fig. 8 Result of Burro9 mesh sensitivity study

320 Increasingly mesh refinements help to resolve maximum concentration more
 321 accurately. The difference of gas concentrations between meshes are significantly

322 reduced with refinement. Due to computational restriction, no further mesh is
 323 used for mesh sensitivity study and Mesh 3 parameters (Table 8) is chosen for the
 324 following study.

325 5.2.3 Ground heat transfer sensitivity study

326 Three different models of heat transfer from the ground are used to study their
 327 effect on the numerical results, which are summarised in Table 9. For constant
 328 heat flux case, the value of 200 W/m^2 is used.

Table 9 Wall thermal boundary conditions in Burro tests

	Case 1	Case 2	Case 3
Heat transfer model	Adiabatic wall	Constant Heat Flux	Wall temperature
Label (Fig. 9)	Adiabatic	fixedFlux	fixedTem

329 The effect of ground heat in predicting peak gas concentration is plotted in
 330 Figure 9.

331 The adiabatic case results in a better prediction of experimental data than
 332 the fixed flux and fixed temperature cases. However, all simulations yield under-
 333 predicted results. This may be due to that the buoyancy effect is over-predicted
 334 and consequently the gas concentration is zero in the fixed flux case at downwind
 335 arcs (at 400 and 800 m).

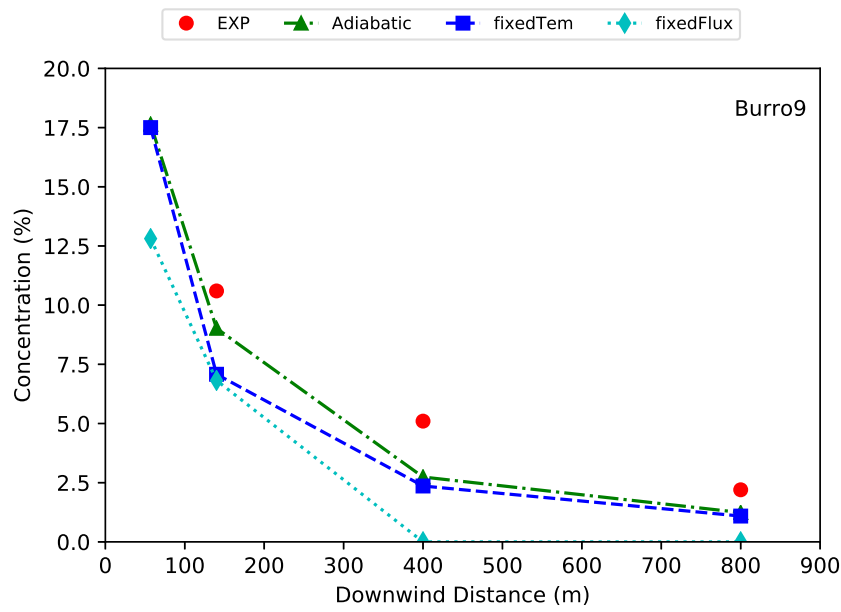


Fig. 9 Result of Burro9 ground heat transfer study

5.2.4 Turbulence Schmidt number, Sc_t , sensitivity study

Two values of $Sc_t = 1$ and $Sc_t = 0.3$ are used for studying the sensitivity of the proposed model in predicting the maximum gas concentration. Results are compared in Figure 10.

$Sc_t = 0.3$, which was used previously in wind tunnel dense gas dispersion is shown to be appropriate for accurate prediction of maximum gas concentration at the 57 m array and 140 m array. Further downwind, at 400 m array and 800 m array, there is no significant difference between the two values.

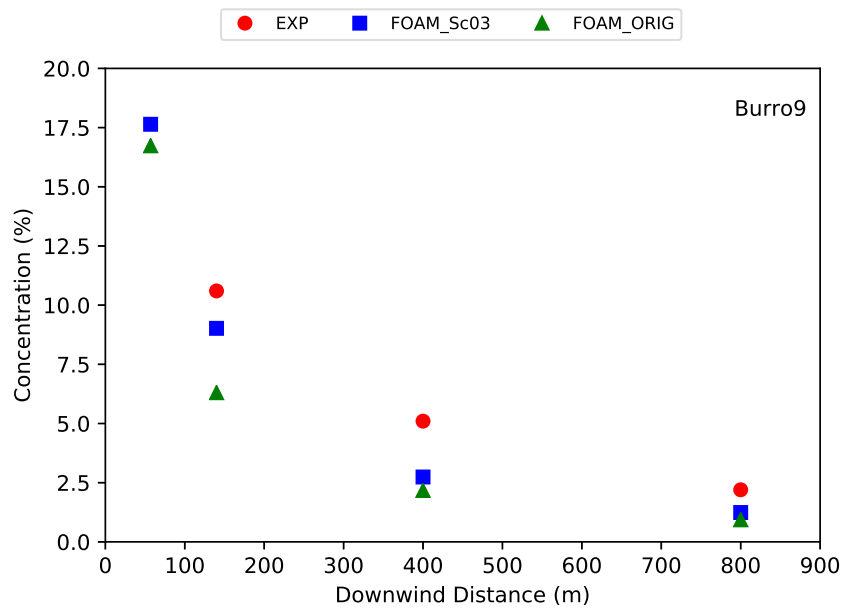


Fig. 10 Result of *Burro9* turbulent Schmidt number Sc_t study

344 5.2.5 Isosurface contour

345 The vertical isosurface contours at $X = 140$ are illustrated in Figure 11. Under-
 346 predicted cloud height are revealed in all tests indicating that the cloud buoyancy
 347 is not correctly solved.

348 Horizontal isosurface contours at height $Z = 1$ are shown in Figure 12. The gas
 349 concentration contour is plotted side by side with the contour from experiment
 350 data, where the left is the result of interpolating concentration at some concen-
 351 tration data points (presented in plots by black dot points), the right is from
 352 experimental data. Overall, the cloud height is considerably well predicted but
 353 the cloud width is over-predicted. Furthermore, it can be seen that the gas moves
 354 downwind slower than experimental data, which under-estimates the downwind
 355 spreading of the gas cloud.

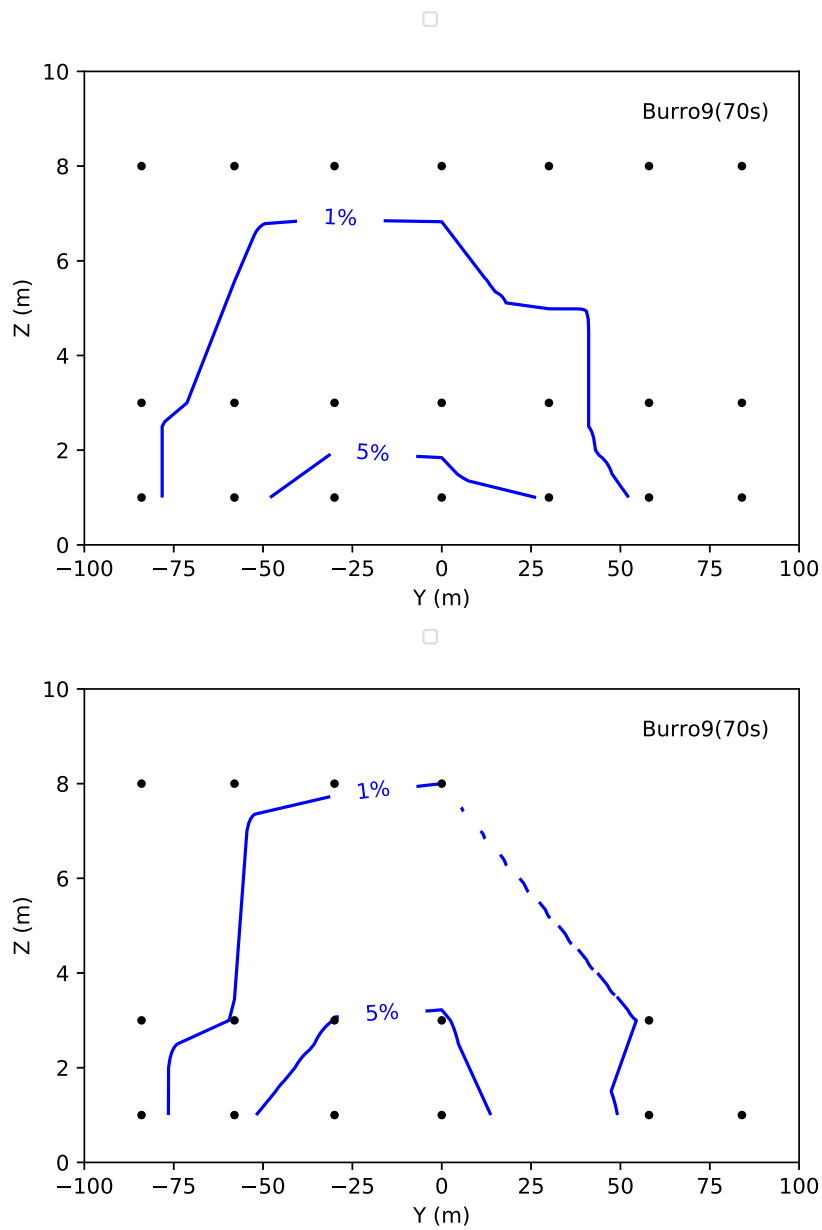


Fig. 11 Vertical isosurface at $X = 140$, Top: Simulation, Bottom: Experimental data of Burro9

test

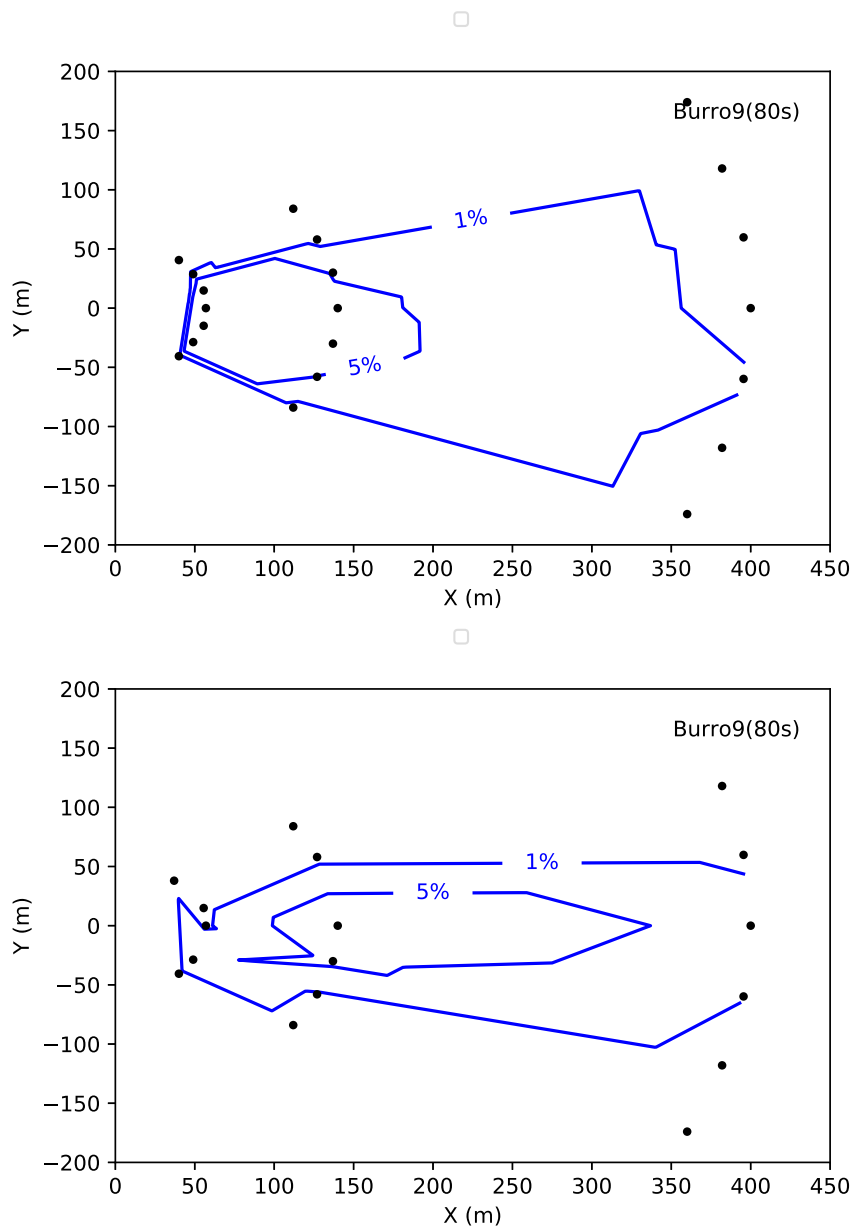


Fig. 12 Horizontal isosurface at $Z = 1$; Top: Simulation, Bottom: Experimental data of Burro9

test

356 5.2.6 Concentration predictions

357 FDS (Fire Dynamics Simulator) (McGrattan et al., 2013) is a low Mach number
358 code using the LES turbulence model. The computational domain is discretised
359 into a connected rectilinear mesh. The governing equations are discretised using
360 finite-difference method. A second-order scheme is used for space discretisation and
361 an explicit second-order Runge-Kutta scheme for time discretisation. OpenFOAM
362 concentration results are compared with FDS data extracted from (Mouilleau and
363 Champassith, 2009).

364 The comparison of OpenFOAM, FDS, and experimental results for **Burro9** test
365 is shown in Figure 13. FDS is over-predicted, while OpenFOAM is under-predicted.
366 However, OpenFOAM is accurate in prediction at 800 m arc.

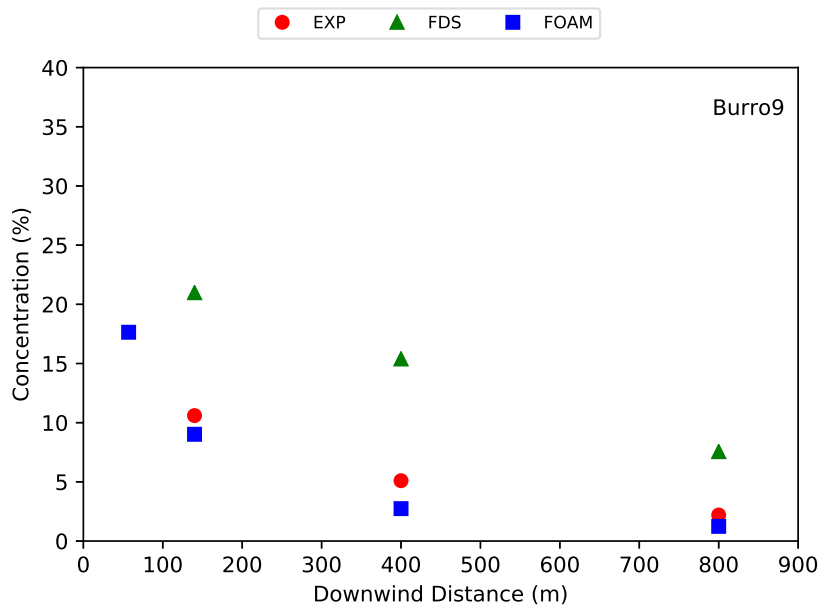


Fig. 13 Maximum arc-wise gas concentrations Burro9 test

367 Figure 14 is the plot of gas concentration at 1 m elevation at 140 m down-
368 wind of Burro9 experiment (EXP) and simulations using the developed solver
369 (FOAM) and FDS (FDS). For the developed solver result, the peak concentra-
370 tion is under-estimated while the temporal trend of changing concentration gen-
371 erally shows good agreement with validation data. The concentration magnitude
372 is fairly matched except during local maximum/minimum durations. Also shown
373 in Figure 14 is the result from FDS simulation which is generally over-predicted.
374 However, the developed solver cannot capture the fluctuation, while FDS yields
375 fluctuating gas concentration over the time period. This is an advantage of LES
376 over RANS turbulence model. The over-prediction of FDS may be due to that a
377 constant coefficient Smagorinsky model was adopted in the simulation. However,
378 the dynamic Smagorinsky model was shown to improve the gas dispersion predic-
379 tion (Ferreira Jr. and Vianna, 2016). This indicates that it would be a promising
380 approach to use LES in order to enhance the performance of the developed solver.

381 *5.2.7 Statistical model evaluation*

382 Overall statistical performance of OpenFOAM results are compared versus FLACS
383 with data extracted from (Hansen et al., 2010) in Table 10. The predictions do
384 not match all SPMs. However, some important SPMs are within the acceptable
385 range. All gas concentrations are within a factor of two (FAC2=1) and better than
386 FLACS (FAC2 = 0.94).

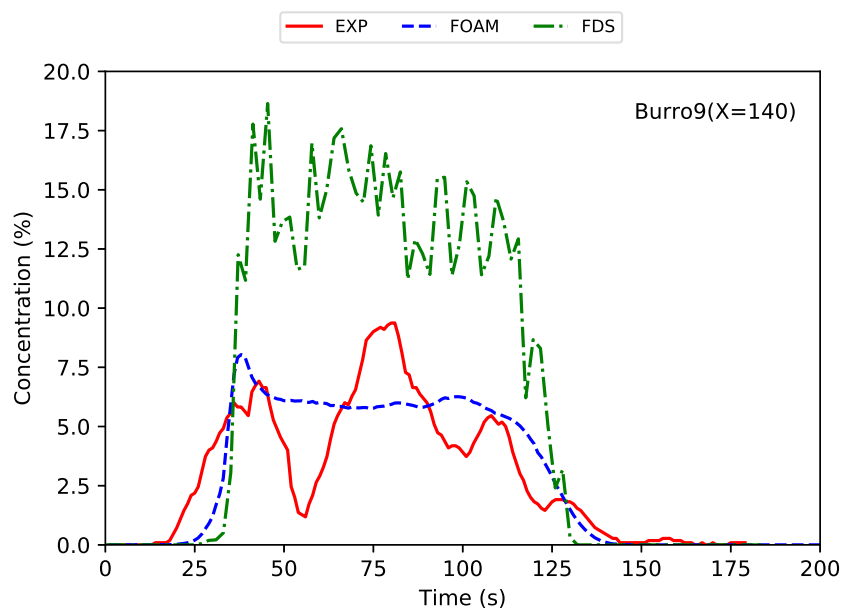


Fig. 14 Point concentration at 140 m of Burro9 test

Table 10 Statistical performance measures of Burro tests

	MRB	RMSE	FAC2	MG	VG
FLACS (Hansen et al., 2010)	0.16	0.12	0.94	1.18	1.14
FOAM Burro9	0.44	0.23	1	0.63	1.28

387 6 Conclusions

388 A solver is developed to reproduce horizontal homogeneous atmospheric surface
 389 layer in neutrally stratified ABL using OpenFOAM. The empirical atmospheric
 390 boundary layer model MOST is used to specify the inlet boundary conditions for
 391 velocity, turbulent kinetic energy and dissipation rate. Flow variable profiles at
 392 outlet boundary are successfully maintained and consistent with their profiles at
 393 the inlet boundary. This demonstrates the effectiveness of the solver in simulating

394 the horizontal homogeneous atmospheric surface layer. It can also predict different
395 levels of ABL turbulence kinetic energy.

396 A solver for ABL gas dispersion simulation taking into account buoyancy ef-
397 fect, variable turbulence Schmidt number and ground heat transfer is developed
398 using the OpenFOAM platform. In the study of dense gas dispersion in neutral
399 simulated ABL, the model is successfully validated by reproducing maximum gas
400 concentration. SPMs from simulation results are better than those from the spe-
401 cialized commercial software for gas dispersion, FLACS.

402 In the study of LNG accidental release, a dense cold gas vapour dispersion in
403 ABL with three ground heat transfer assumptions are simulated and compared
404 with the full scale field measurements. The gas peak concentration is used as val-
405 idation parameters. Adiabatic wall assumes zero heat flux from ground to the gas
406 cloud, whereas, the fixed temperature model assumes isothermal ground where the
407 ground temperate remains unchanged when in contact with the cold gas cloud. The
408 real heat flux to the gas cloud would be in between these two cases. The other
409 model assuming a fixed flux of heat to the gas cloud is also included. Of the three
410 ground heat transfer models, adiabatic wall gives the closest prediction of gas
411 peak concentration. The model is shown to accurately predict vertical buoyancy
412 while the cloud spreading downwind is under-predicted. SPMs from the simula-
413 tion results are compared with the LES code FDS and specialized dispersion code
414 FLACS, showing that the solver is more accurate in predicting gas concentra-
415 tion in neutrally stratified ABL. Further investigation is required to validate the
416 OpenFOAM solver in ABL with thermal stratification.

References

- 417 **References**
- 418 Ferreira Jr ES, Vianna SSV (2016) LARGE EDDY SIMULATION COMBINED
419 WITH EQUIVALENT DIAMETER FOR TURBULENT JET MODELLING
420 AND GAS DISPERSION
- 421 Fiates J, Vianna SSV (2016) Numerical modelling of gas dispersion us-
422 ing OpenFOAM. *Process Safety and Environmental Protection* 104,
423 Part:277–293, DOI <http://doi.org/10.1016/j.psep.2016.09.011>, URL
424 <http://www.sciencedirect.com/science/article/pii/S0957582016302105>
- 425 Fiates J, Santos RRC, Neto FF, Francesconi AZ, Simoes V, Vianna SSV (2016) An
426 alternative CFD tool for gas dispersion modelling of heavy gas. *Journal of Loss*
427 *Prevention in the Process Industries* 44:583–593, DOI 10.1016/j.jlp.2016.08.002,
428 URL [https://www.scopus.com/inward/record.uri?eid=2-s2.0-](https://www.scopus.com/inward/record.uri?eid=2-s2.0-84994155203&doi=10.1016%2Fj.jlp.2016.08.002&partnerID=40&md5=f15971c9c9332b320e618d86adf80351)
429 [84994155203&doi=10.1016%2Fj.jlp.2016.08.002&partnerID=40&md5=f15971c9c9332b320e618d86adf80351](https://www.scopus.com/inward/record.uri?eid=2-s2.0-84994155203&doi=10.1016%2Fj.jlp.2016.08.002&partnerID=40&md5=f15971c9c9332b320e618d86adf80351)
- 430 Flores F, Garraud R, Muñoz RC (2013) CFD simulations of
431 turbulent buoyant atmospheric flows over complex geometry:
432 Solver development in OpenFOAM. *Computers & Fluids* 82:1–
433 13, DOI <http://dx.doi.org/10.1016/j.compfluid.2013.04.029>, URL
434 <http://www.sciencedirect.com/science/article/pii/S0045793013001795>
- 435 Foken T (2006) 50 Years of the Monin–Obukhov Similarity Theory. *Boundary-*
436 *Layer Meteorology* 119(3):431–447, DOI 10.1007/s10546-006-9048-6, URL
437 <https://doi.org/10.1007/s10546-006-9048-6>
- 438 Greenshields CJ (2017) OpenFOAM user guide version 5. URL
439 <https://cfd.direct/openfoam/user-guide/>

- 440 Hansen OR, Gavelli F, Ichard M, Davis SG (2010) Validation of FLACS against ex-
441 perimental data sets from the model evaluation database for LNG vapor disper-
442 sion. *Journal of Loss Prevention in the Process Industries* 23(6):857–877, DOI
443 10.1016/j.jlp.2010.08.005, URL <http://dx.doi.org/10.1016/j.jlp.2010.08.005>
- 444 Hargreaves D, Wright N (2007) On the use of the k-epsilon model
445 in commercial CFD software to model the neutral atmospheric
446 boundary layer. *Journal of Wind Engineering and Industrial Aero-
447 dynamics* 95(5):355–369, DOI 10.1016/j.jweia.2006.08.002, URL
448 <http://www.sciencedirect.com/science/article/pii/S016761050600136X>
449 <http://linkinghub.elsevier.com/retrieve/pii/S016761050600136X>
- 450 Ivings MJ, Lea CJ, Webber DM, Jagger SF, Coldrick S (2013) A protocol for
451 the evaluation of LNG vapour dispersion models. *Journal of Loss Prevention
452 in the Process Industries* 26(1):153–163, DOI 10.1016/j.jlp.2012.10.005, URL
453 <http://dx.doi.org/10.1016/j.jlp.2012.10.005>
- 454 Jonathon S, Christian M (2012) k-epsilon simulations of the neutral atmospheric
455 boundary layer: analysis and correction of discretization errors on practical grids.
456 *International Journal for Numerical Methods in Fluids* 70(6):724–741, DOI
457 doi:10.1002/fld.2709, URL <https://doi.org/10.1002/fld.2709>
- 458 Jones WP, Launder BE (1972) The prediction of laminarization with a two-
459 equation model of turbulence. *International Journal of Heat and Mass Trans-
460 fer* 15(2):301–314, DOI [https://doi.org/10.1016/0017-9310\(72\)90076-2](https://doi.org/10.1016/0017-9310(72)90076-2), URL
461 <http://www.sciencedirect.com/science/article/pii/0017931072900762>
- 462 Launder BE, Spalding DB (1974) The numerical computation of tur-
463 bulent flows. *Computer Methods in Applied Mechanics and Engineer-
464 ing* 3(2):269–289, DOI [http://dx.doi.org/10.1016/0045-7825\(74\)90029-2](http://dx.doi.org/10.1016/0045-7825(74)90029-2), URL

- 465 <http://www.sciencedirect.com/science/article/pii/0045782574900292>
- 466 Luketa-Hanlin A, Koopman RP, Ermak DL (2007) On the application of com-
467 putational fluid dynamics codes for liquefied natural gas dispersion. *Journal of*
468 *Hazardous Materials* 140(3):504–517, DOI 10.1016/j.jhazmat.2006.10.023
- 469 Mack A, Spruijt MPN (2013) Validation of OpenFoam for heavy gas dis-
470 persion applications. *Journal of Hazardous Materials* 262:504–516, DOI
471 10.1016/j.jhazmat.2013.08.065
- 472 McGrattan K, Hostikka S, McDermott R, Floyd J, Weinschenk C, Overholt K
473 (2013) Fire dynamics simulator, user’s guide. NIST special publication 1019:20
- 474 Mouilleau Y, Champassith A (2009) CFD simulations of at-
475 mospheric gas dispersion using the Fire Dynamics Simulator
476 (FDS). *Journal of Loss Prevention in the Process Industries*
477 22(3):316–323, DOI <https://doi.org/10.1016/j.jlp.2008.11.009>, URL
478 <http://www.sciencedirect.com/science/article/pii/S0950423008001496>
- 479 Nielsen M, Ott S (1996) A collection of data from dense gas experiments. Tech.
480 rep., Risø National Laboratory, Roskilde
- 481 Parente A, Gorré C, van Beeck J, Benocci C (2011) Improved k-epsilon
482 model and wall function formulation for the RANS simulation of
483 ABL flows. *Journal of Wind Engineering and Industrial Aerodynam-*
484 *ics* 99(4):267–278, DOI <https://doi.org/10.1016/j.jweia.2010.12.017>, URL
485 <http://www.sciencedirect.com/science/article/pii/S016761051100002X>
- 486 Pontiggia M, Derudi M, Busini V, Rota R (2009) Hazardous gas dispersion:
487 A CFD model accounting for atmospheric stability classes. *Journal of haz-*
488 *ardous materials* 171(1-3):739–747, DOI 10.1016/j.jhazmat.2009.06.064, URL
489 <http://www.sciencedirect.com/science/article/pii/S0304389409009844>

- 490 Richards PJ, Hoxey RP (1993) Appropriate boundary conditions for
491 computational wind engineering models using the k-epsilon turbulence
492 model. *Journal of Wind Engineering and Industrial Aerodynamics* 46-
493 47(Supplement C):145–153, DOI [https://doi.org/10.1016/0167-6105\(93\)90124-](https://doi.org/10.1016/0167-6105(93)90124-7)
494 7, URL <http://www.sciencedirect.com/science/article/pii/0167610593901247>
- 495 Richards PJ, Norris SE (2011) Appropriate boundary conditions for computational
496 wind engineering models revisited. *Journal of Wind Engineering and Industrial*
497 *Aerodynamics* 99(4):257–266, DOI <https://doi.org/10.1016/j.jweia.2010.12.008>,
498 URL <http://www.sciencedirect.com/science/article/pii/S0167610510001418>
- 499 Yan BW, Li QS, He YC, Chan PW (2016) RANS simulation of neutral atmospheric
500 boundary layer flows over complex terrain by proper imposition of boundary
501 conditions and modification on the k-epsilon model. *Environmental Fluid Me-*
502 *chanics* 16(1):1–23, DOI 10.1007/s10652-015-9408-1
- 503 Yang Y, Gu M, Chen S, Jin X (2009) New inflow boundary conditions for
504 modelling the neutral equilibrium atmospheric boundary layer in computa-
505 tional wind engineering. *Journal of Wind Engineering and Industrial Aerody-*
506 *namics* 97(2):88–95, DOI <http://dx.doi.org/10.1016/j.jweia.2008.12.001>, URL
507 <http://www.sciencedirect.com/science/article/pii/S0167610508001815>

2019-08-02

CFD simulation of dense gas dispersion in neutral atmospheric boundary layer with OpenFOAM

Tran, Vu

Springer

Tran V, Ng EYK, Skote M. (2019) CFD simulation of dense gas dispersion in neutral atmospheric boundary layer with OpenFOAM. *Meteorology and Atmospheric Physics*, Volume 132, April 2020, pp. 273-285

<https://doi.org/10.1007/s00703-019-00689-2>

Downloaded from Cranfield Library Services E-Repository